Available online at www.sciencedirect.com
ScienceDirect
Biochemical and Biophysical Research Communications 349 (2006) 79–90
BBRC
www.elsevier.com/locate/ybbrc

Crystal structure of rubredoxin from *Desulfovibrio gigas* to ultra-high 0.68 Å resolution ☆

Chun-Jung Chen [a,b,*], Yi-Hung Lin [a], Yen-Chieh Huang [a], Ming-Yih Liu [a,c,*]

[a] *Life Science Group, Research Division, National Synchrotron Radiation Research Center, Hsinchu 30076, Taiwan*
[b] *Department of Physics, National Tsing-Hua University, Hsinchu 30043, Taiwan*
[c] *Department of Biological Science and Technology, National Chiao Tung University, Hsinchu 30045, Taiwan*

Received 27 July 2006
Available online 11 August 2006

Abstract

Rubredoxin (*D.g.* Rd) is a small non-heme iron–sulfur protein shown to function as a redox coupling protein from the sulfate reducing bacteria *Desulfovibrio gigas*. The protein is generally purified from anaerobic bacteria in which it is thought to be involved in electron transfer or exchange processes. Rd transfers an electron to oxygen to form water as part of a unique electron transfer chain, composed by NADH:rubredoxin oxidoreductase (NRO), rubredoxin and rubredoxin:oxygen oxidoreductase (ROO) in *D.g.* The crystal structure of *D.g.* Rd has been determined by means of both a Fe single-wavelength anomalous dispersion (SAD) signal and the direct method, and refined to an ultra-high 0.68 Å resolution, using X-ray from a synchrotron. Rd contains one iron atom bound in a tetrahedral coordination by the sulfur atoms of four cysteinyl residues. Hydrophobic and π–π interactions maintain the internal Rd folding. Multiple conformations of the iron–sulfur cluster and amino acid residues are observed and indicate its unique mechanism of electron transfer. Several hydrogen bonds, including N—H···SG of the iron–sulfur, are revealed clearly in maps of electron density. Abundant waters bound to C—O peptides of residues Val8, Cys9, Gly10, Ala38, and Gly43, which may be involved in electron transfer. This ultra-high-resolution structure allows us to study in great detail the relationship between structure and function of rubredoxin, such as salt bridges, hydrogen bonds, water structures, cysteine ligands, iron–sulfur cluster, and distributions of electron density among activity sites. For the first time, this information will provide a clear role for this protein in a strict anaerobic bacterium.

Keywords: Rubredoxin; *Desulfovibrio gigas*; Redox; Crystal structure; Ultra-high resolution; Multiple conformations

Rubredoxin (Rd) is one of the simplest and smallest redox coupling proteins, being somewhat larger than desulforedoxin (Dx), and contains an electron transfer chain from pyridine nucleotides to molecular oxygen. Many rubredoxins have been isolated from various bacteria, including sulfate-reducing bacteria such as *Desulfovibrio* (*D.*) *gigas*, *D. vulgaris*, and *D. desulfuricans* [1–4] or other anaerobes such as *Clostridium thermoaceticum* or *Acetobacter woodii* [5]. They have been found also in aerobic bacteria, i.e., *Acinetobacter calcoaceticus* [6] and *Pseudomonas oleovorans* [7,8]. Most rubredoxins comprise 45–54 amino acid residues, typically 52–55 amino acids, with molecular weights ranging from 5000 to 6000 Da, and contain one iron atom tetrahedrally ligated by four cysteine residues as an active site [4]. Some organisms such as *Pseudomonas oleovorans*, however, contain a Rd with a larger molecular weight, 19,500 Da [4,7]. The iron center of Rd from sulfate-reducing bacteria can be reversibly reduced at a redox potential near 0 mV and in dissimulatory sulfate reduction requires a redox potential between −400 and −200 mV [9,10]. Although several rubredoxins have been found and isolated from various bacteria, 13 of them have had their amino acid sequence delineated and have been found to have sets of the C-X-X-C-G sequence about the iron

☆ *Abbreviations:* Rd, rubredoxin; *D.g.*, *Desulfovibrio gigas*.

* Corresponding authors. Fax: +886 3 578 3813 (C.-J. Chen); +886 3 578 3813 (M.-Y. Liu).
E-mail addresses: cjchen@nsrrc.org.tw (C.-J. Chen), mingliu@nsrrc.org.tw (M.-Y. Liu).

0006-291X/$ - see front matter © 2006 Elsevier Inc. All rights reserved.
doi:10.1016/j.bbrc.2006.07.205

center [11]. The physiological role of Rd in most microbials remains unclear, although Rds from *C. thermoaceticum* and *Acetobacterium woodii* were found to serve as electron acceptors for CO dehydrogenase [5], and a *C. perfringens* was reported to be involved in the reduction of nitrate to ammonia with NAD(P)H [3]. An additional role as a cofactor in hydrogen oxidation in *Azotobacter vinelandii* has also been described [12].

The sulfate-reducing bacteria (SRB) *Desulfovibrio gigas* (*D. gigas*), a strict anaerobe, contains a well-characterized metabolic pathway, the so-called Embden–Meyerhof–Parnas pathway, that enables it to survive transient contacts with oxygen [13]. *D. gigas* has been well-studied in terms of a search for its electron-transfer partners and the function of rubredoxin. This is the only rubredoxin from a strict anaerobe for which a physiological role has been fully delineated: it is an intermediate in the electron transfer chain that allows *D. gigas* to utilize polyglucose in the presence of oxygen, as Santos et al., demonstrated [14]. Rubredoxin transfers electrons to oxygen to form water as part of a unique electron-transfer chain, comprising NADH:rubredoxin oxidoreductase (NRO) [15] and rubredoxin:oxygen oxidoreductase (ROO) [16–18] in *D. gigas*, as shown in Scheme 1 [14]. NRO can induce the specific reduction of *D. gigas* Rd and shows low reaction rates with Rd from other *Desulfovibrio*. This enzyme is composed of two subunits, of molecular weight 27 and 32 kDa, and contains both FAD and riboflavin 5′-phosphate (FMN) [15], but Rd found in *D. vulgaris Hildenborough* cells, for which no NRO activity is detected, might have further physiological roles. ROO, a homodimer of molecular weight 43 kDa per monomer, acts physiologically as the electron acceptor for *D. Gigas* Rd [16]. This three-component soluble electron-transfer chain couples NADH oxidation with oxygen reduction to water, allowing simultaneously for NAD^+ regeneration and oxygen utilization.

More than 20 rubredoxin structures are deposited in the protein data bank (PDB). Crystal structures of rubredoxin were earlier reported for proteins from *Clostridium* (*C.*) *pasteurianum* [19] at 2.5 Å resolution, *D. vulgaris* and *D. gigas* both at 1.5 Å resolution [20]. Later refined, the structures of rubredoxins for each organism at highest resolution have been reported from *C. pasteurianum* at 1.1 Å [21], *D. gigas* at 1.4 Å [22], *D. desulfuricans* (ATCC 27774) at 1.5 Å [23] *D. vulgaris* at 1.0 Å resolution [24], and *P. furiosus* at 0.95 Å [25] for which the highest resolution approaches the border of 1.0 Å, and *P. abyssi* mutants at resolution 0.69 Å resolution [26]. A comparison of these rubredoxin crystal structures provides the possibility to determine general rules about their sites of activity and recognition with other redox partners, i.e., NRO, ROO, etc.

Here we report the Rd structure from the crystals well-diffracted at ultra-high resolution 0.68 Å to push the limit of the boundary between proteins and small molecules. This ultra high-resolution structure allows us to study the structure of rubredoxin in great detail and to reveal the remaining puzzle of its biological functions, such as salt bridges, hydrogen bonds, water structures, cysteine ligands, iron–sulfur cluster, and distribution of electron density among activity sites. This information provides for the first time a clear role for this protein in a strictly anaerobic bacterium.

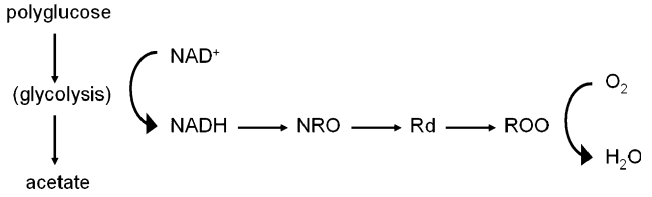

Scheme 1.

Materials and methods

Protein purification, crystallization and X-ray data collection. Desulfovibrio gigas (ATCC 19364) was grown as previously described [27]. Rubredoxin was purified from *D. gigas* under anaerobic condition described by Sieker et al. [4]. The crystallization method and conditions have been reported [28]. Crystallization was achieved by the hanging-drop vapor-diffusion method using ammonium sulfate as the precipitant with an acidic buffer of pH 4.0 and 23 °C. X-ray diffraction data were collected at both beamlines BL13B at National Synchrotron Radiation Research Center (NSRRC) in Taiwan and BL12B2 (Taiwan-contracted beamline) at SPring-8 in Japan. The final data of ultra-high resolution 0.68 Å were processed and merged using *HKL2000* [29] from two rotations with one medium-high resolution range (25–1.2 Å) and the other with medium-high to ultra-high resolution (1.8–0.68 Å), and were 92.6% complete with $R_{merge} = 7.3\%$ to 0.68 Å. The crystals belong to space group $P2_1$ with unit-cell dimensions of $a = 19.44$ Å, $b = 41.24$ Å, $c = 24.10$ Å, and $\beta = 108.46°$. Details of data statistics appear in Table 1.

Structural determination and refinement. Despite the *D. gigas* Rd structure being previously determined at 1.4 Å resolution [22], we collected the iron-anomalous dispersion signal with the peak wavelength 1.7389 Å to redetermine the structure *ab inito*, so as to perform a non-biased refinement of the structure at ultrahigh-resolution. The anomalous-difference Patterson map shows a clear resolution of the iron atom corresponding to the [Fe-4S] cluster. The single Fe site was determined and directed to the program *SOLVE 2.01* [30] for phase calculation using single-wavelength anomalous dispersion (SAD). With density modification and auto-model building in the *RESOLVE* program [30], the electron density is clearly interpretable, and the Rd structure was completely determined at 2.0 Å within 2 h (SGI O2+ computer). Because data were collected at ultrahigh-resolution, the structure was also determined by direct method using *SHELXE* [31] at 0.9 Å resolution; the structures from the two methods are closely similar.

CNS v1.1. [32], *SHELX97* [31], and *O* [33] (Jones et al., 1991) programs were used for refinement and model building with manual adjustment, respectively. A randomly selected 4949 reflections (5% of the total observed reflections) in the full-resolution range (10–0.68 Å) were used as a test set for calculation of the free *R*-factor. The preliminary structure from Fe-SAD was initially directed into a rigid body refinement with data 15–2.0 Å by *CNS v.1.1.*, giving $R = 0.2656$ and $R_{free} = 0.2787$. The model was then refined with rigid-body fitting in the resolution range 10–1.0 Å using *SHELX97*, which gave $R = 0.2656$ and $R_{free} = 0.2787$. After verifying the map and minor adjustments of the model, several cycles of isotropic refinement in the resolution range 10–1.0 Å yielded decreased to $R = 0.1931$and $R_{free} = 0.2059$. Then solvent molecules were automatically introduced into the model structure with *SHELXWAT* [31] with a temperature *B*-factor cutoff 50 $Å^2$. At this stage, the *R* became 0.1317 and $R_{free} = 0.1568$. Further refinement was performed with conjugate-gradient least-squares minimization with anisotropic *B* factors and all data (10–0.68 Å) included, resulting in $R = 0.1121$ and $R_{free} = 0.1346$. The riding

Table 1
Data collection statistics and refinement

	SPring-8, BL12B2
Crystal data collection	
Wavelength (Å)	0.689
Temperature (K)	110
Space group	$P2_1$
Unit-cell parameters (Å)	
a (Å)	19.44
b (Å)	41.24
c (Å)	24.10
β (°)	108.46
Resolution range (Å)	25–0.68 (0.75–0.68)
No. of unique reflections	52,365
Completeness (%)	92.6 (57.1)
$\langle I/\sigma_{(I)}\rangle$	24.2 (3.6)
Average redundancy	16.6
$R_{sym}(I)$ (%)[a]	7.3 (26.1)
Mosacity (°)	0.346
No. of proteins/A.U.	1
Refinement and model statistics	
Resolution range (Å)	10–0.68
Number of reflections	47,119
Number of observed reflections[b]	45,181
Number of total non-hydrogen atoms	400
Number of solvents	101
R_{work} (%)[c]	9.91
R_{free} (%)[d]	11.07
Average B-factor (Å^2)	7.55
Minimum B-factor (Å^2)	3.90
Maximum B-factor (Å^2)	41.27
R.m.s. deviation from ideal values	
Bond length (Å)	0.016
Bond angles (°)	1.874
Dihedral angles (°)	23.985
Improper torsion angles (°)	1.003
Estimated coordinate error	
Low-resolution cutoff (Å)	5.0
ESD from Luzzati plot (Å)[e]	0.03
ESD from SIGMAA (Å)[e]	0.29
Ramachandran outliers (%)[f]	0

[a] $R_{sym} = \sum_h \sum_i [|I_i(h) - \langle I(h)\rangle|/\sum_h \sum_i I_i(h)]$, where I_i is the ith measurement and $\langle I(h)\rangle$ is the weighted mean of all measurements of $I(h)$.

[b] Reflections of $4\sigma_I$ cutoff were applied in generating the refinement statistics.

[c] $R_{work} = \sum_h |F_o - F_c|/\sum_h F_o$, where F_o and F_c are the observed and calculated structure factor amplitudes of reflection h.

[d] R_{free} is as R_{work}, but calculated with 10% of randomly chosen reflections omitted from the refinement.

[e] ESD, estimated standard deviation.

[f] Ramachandran plot outliers are all glycines.

hydrogen atoms (C—H and N—H) were then located automatically with *SHELX97*, but their coordinates were not refined. The introduction of the riding H atoms to the model yielded $R = 0.0996$ and $R_{free} = 0.1167$. After several cycles of manual adjustment and refinement, multiple conformations of various amino acid residues and several additional water molecules were added to the model, which was subjected to a final step of one cycle of full-matrix least-squares minimization. The detailed refinement procedure and statistics are given in Table 2. In this refinement, the L.S. and BLOC commands were combined to perform the least-squares calculation [31]. The maximum shifts in atom positions were 0.03 and 0.165 Å, and the maximum shifts of the B factors were 0.47 and 17.7 Å^2, for non-H atoms and solvent atoms, respectively. The highest and deepest peaks in the final $|F_o - F_c|$ difference map were 0.65σ and -0.99σ, respectively. The final model was evaluated with *PROCHECK* [34]. Statistics of the structure refinement appear in Table 1.

Table 2
Detail refinement procedure of Rd structure

SHELX-97 refinement

Action taken	R_1 (%)	R_{free} (%)
Rigid body (10–1.0 Å) (input from *CNS*)	25.56	27.87
Coordinates and isotropic B-factors (10–1.0 Å)	19.31	20.59
First model rebuilding and adjustments	15.24	17.09
Preliminary water structures (56 H_2O)	13.17	15.68
Model adjustments and 13.01	15.46	
Include all data (10–0.68 Å)	13.92	15.78
All atom anisotropic	11.21	13.46
Model adjustments	11.08	13.02
More water structure added (101 H_2O)	10.54	12.25
Ride hydrogens added	9.96	11.67
Minor adjustments	9.91	11.07

No. of non-hydrogen atoms: 400 + 101 (solvents).
4612 parameters refined (positional, occupancies and anisotropic B-factors).
Reflection used: $R1$: 45,181, R_{free}: 5023 ($F_o > 4\sigma$).

Result and discussion

Structural quality and validation

The refined structural model of *D.g.* Rd at 0.68 Å resolution gave R factors of 0.1031 and 0.0991 for all observed 47119 ($I > 0$) and 45181 ($I > 4\sigma_I$) reflections, respectively. The ratio of reflections to parameters is greater than 10 (47119/4612), which provides confident in the free-atom refinement. The corresponding R_{free} factors for 5239 (~10%) randomly selected test-set reflections and for those 5023 with $I > 4\sigma_I$ were 0.1133 and 0.1107, respectively, according to the *SHELX97* refinement protocol (Table 2). The final model contains complete 52 residues, one iron atom, and 101 water molecules. The anisotropic temperature factors employed for all atoms, including all solvent atoms, and for alternative conformations of the protein decreased the R-factor by 4–5%. Furthermore, the positioning of riding H atoms reduced the R-factor by ~0.5 % as hydrogen atoms account for about one seventh of the molecular weight of the molecule. No H atoms were generated for water molecules, although they were in some cases identified in the $|F_o - F_c|$ maps. The root-mean-square (r.m.s.) deviations of the final model from ideal geometry were 0.016 Å for the bond lengths and 1.874° for bond angles. The mean error in atomic positions as estimated with a Luzzati [35] plot is about 0.03 Å (5.0–0.68 Å resolution range) (Fig. 1a). The stereochemistry test showed that 95% and 5% (two residues, one for Cys9 with $\Phi = -132.36^\circ$ and $\Psi = 10.77^\circ$ and another for Asp19 with $\Phi = -157.26^\circ$ and $\Psi = 77.76^\circ$) of the residues were located in the most favored and additional allowed regions of the Ramachandran plot, respectively (Fig. 1b). In the final model, the anisotropic B factors of atoms ranged from 3.9 to 41.3 Å^2 and the mean B factor was 7.55 Å^2

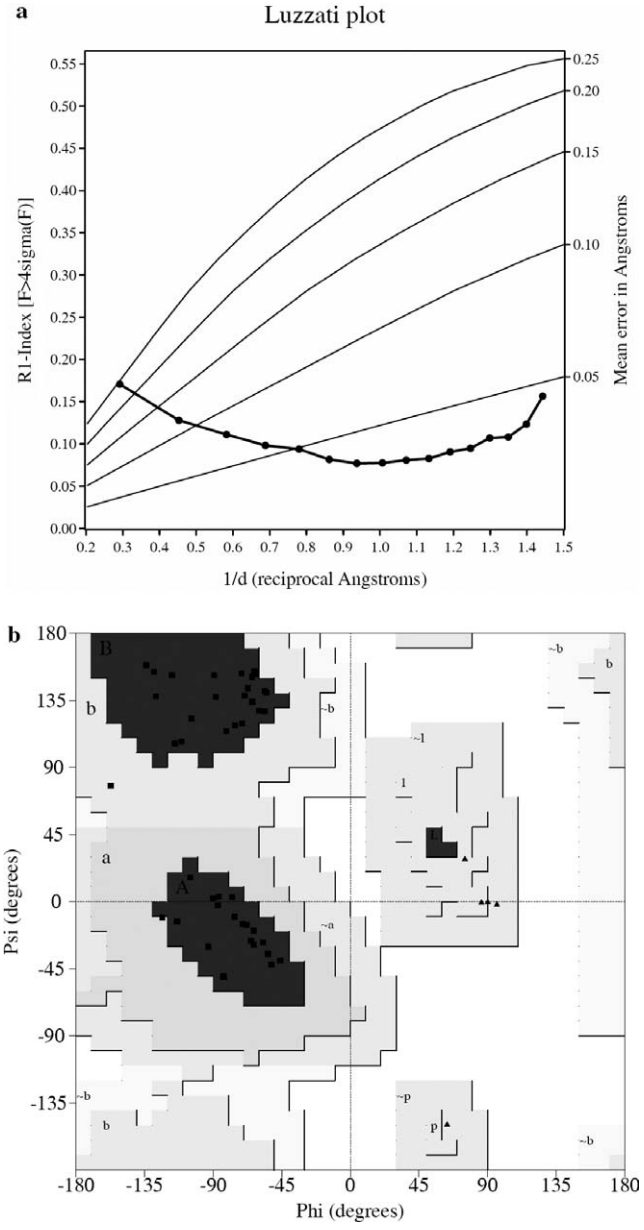

Fig. 1. (a) Observed and theoretical (Luzzati, 1952) variation in the *R* factor *versus* 1/d. The five thin lines correspond to the theoretical variations when only coordinate errors of the model (0.25, 0.20, 0.15, 0.10, 0.05 Å) contribute to the difference between observed and calculated structure factors. (b) Ramachandran plot of ϕ-ψ after refinement.

(Fig. 2). The iron and sulfur atoms of the iron–sulfur cluster had a least mean *B* factor 4.27 Å^2, and their maximum shifts in both coordinates and *B* factors were the least (<0.001 Å and 0.008 Å^2, respectively) in the final full-matrix least-squares refinement.

Residue properties and structure geometries

The map of electron density at ultrahigh-resolution allowed us to describe the essential structural features of the residues and solvents with great certainty. The atoms of the protein that are less well-defined ($B > 20$ Å^2) are Met1, Asp2, and Gln52 of the N and C termini and the extremities of Glu12, Glu31 and all the lysine residues, except Lys46. The largest deviation of main-chain bond lengths (C—N) found between Met1 and Asp2 is 0.051 Å larger than the ideal 1.329 Å. Three major absolute deviations from the mean of omega torsion angle found for Glu12 (13.59°), Val41 (11.73°), and Asp47 (13.75°) probably reflect local disorder. One extreme absolute deviation from mean Chi-1 value was found for Lys25 (47.26°), which is involved in hydrogen bonds and contacts with three neighboring molecules. The notable r.m.s. distance from planarity were observed at residue Tyr13 (0.043 Å) [36]. The maximum main-chain bond lengths (1.380 Å) differing from small-molecular values (1.329 Å) occurred at the C—N bond between Met1 and Asp2. Three residues with a *cis*-peptide conformation were found for Val5, Pro15, and Pro34.

Structural model

The protein structure contains all 52 residues with the iron atom bound in a tetrahedral coordination by the sulfur atoms of four cysteinyl residues (Fig. 3a). The folding consists basically of two major single-stranded single loops (Ile3 to Tyr15) and (Asp36 to Lys46) and a twisted loop (Pro16 to Gly27). It is stabilized by a core of side-chains of nearly invariant hydrophobic or aromatic residues–Tyr4, Tyr11, Tyr13, Phe30, Trp37, and Phe49 of which Tyr4 and Phe30 form π–π interactions (Fig. 4). The framework of hydrogen bonds involving main-chain atoms, invariant side-chain atoms, and various water molecules contributes greatly to the structural stability (Fig. 5). This specific core arrangement appears to be essential for the integrity of the metalloprotein structure and probably plays a role in controlling or stabilizing the redox states of a metal center of this type. A possible role of the aromatic core is to mediate a long-range electron transfer, through π–π interactions, between the redox center and a functional partner, which would interact with rubredoxins on the opposite side of the molecule. The detailed secondary structure comprises a small three-stranded pleated sheet (Tyr4 to Cys6; Glu12 to Tyr13; and Phe49 to Lys51) and numerous tight turns, of which some turns form short "helical corners", which allow the chain to turn approximately 90°: Pro15 to Lys17, Asp19 to Asp21, Phe30 to Asp32, and Lys46 to Ala48. The first turn of each of these helical corners is identical with the 3_{10} helix and the second is of the hairpin type-I bend [37]. The geometries of hydrogen bonds are comparable to those found in previous highly refined Rd model [22]. The conservation of the overall architecture of rubredoxin, especially the hydrophobic core and the strong network of hydrogen bonds, reflects its great stability and remarkable ability to crystallize well. In RdDg, Lys25 is involved in intermolecular contacts with three nearest neighbors of symmetry-related molecules. This condition is a consequence of hydrogen bonding between this residue and residue Asp47 on the other hand of symmetry-related molecule, and between this residue

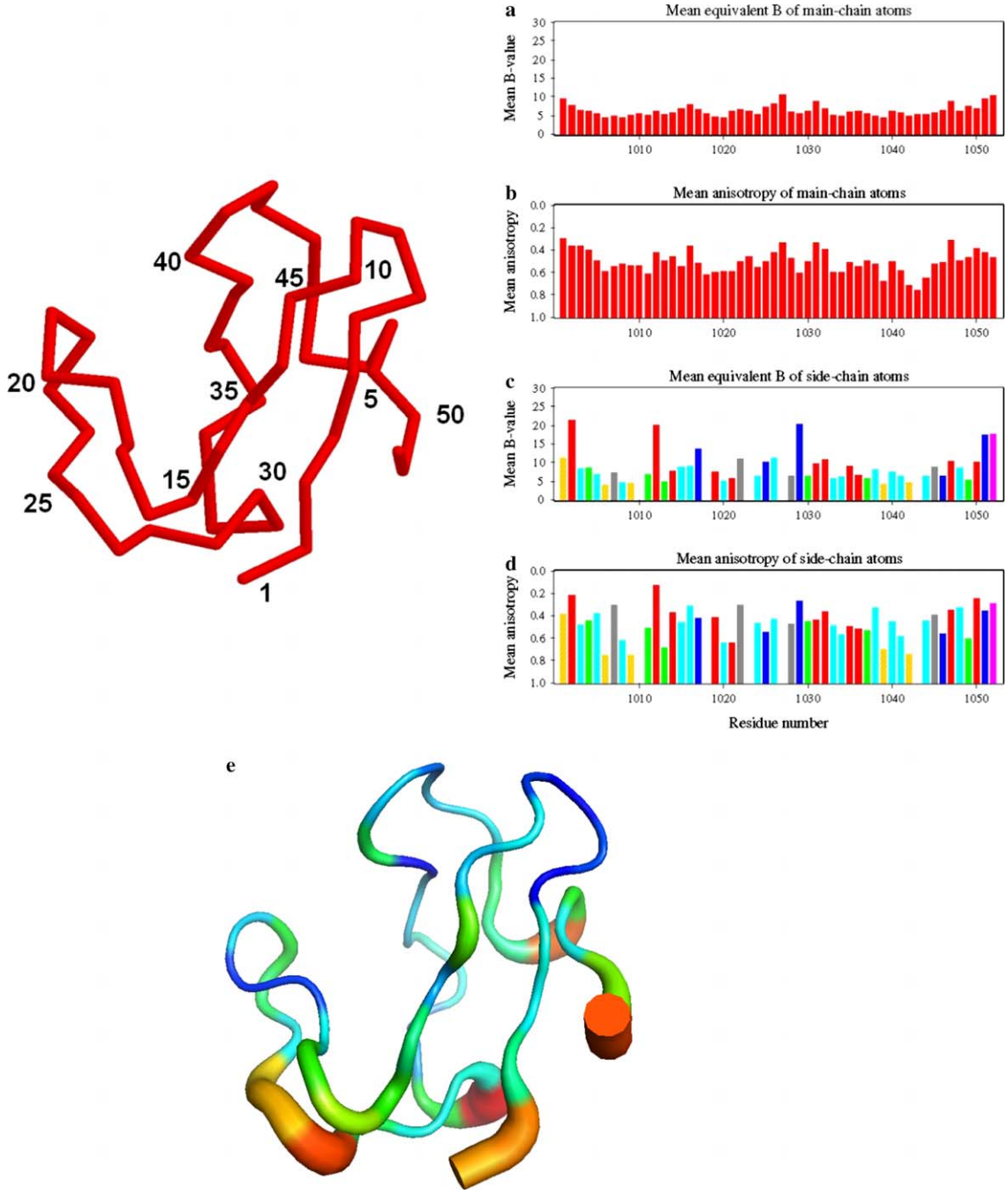

Fig. 2. Distribution of the temperature factor of Rd structure. (a) Main equivalent temperature factors (*B*-values) of main-chain atoms. (b) Mean anisotropy of main-chain atoms. (c) Main equivalent *B* values of side-chain atoms. (d) Mean anisotropy of side-chain atoms. (e) Temperature-factor puttied structure.

and the peptide carbonyl O40 on the other symmetric molecule. Also of interest is that no lysine residues exposed to solvent—Lys17, Lys29, and Lys51—are involved in the molecular packing. In all structures, the quasi-invariant hydrophobic region enclosing the FeSG4 array is delimited by a ring of acidic residues, which are either partially involved in the structural internal hydrogen bonds as mentioned above (Asp14, Asp19) or fully exposed to the solvent (Glu12, Asp21, Asp35, Asp36, Asp47, and Glu50). All remaining charged residues lie on the other side of the molecule, away from the redox center. It is notable that Asp35 and Asp47 possibly share a proton.

Comparison with the 1.4 Å structure

The overall structure has essentially the same fold as the room-temperature structure at 1.4 Å resolution (Frey et al, 1984), but significant differences exist at the N, C-terminus and in the region around residues Asp35 (Fig. 3b). In contrast to the 1.4 Å resolution structure, the present ultra-

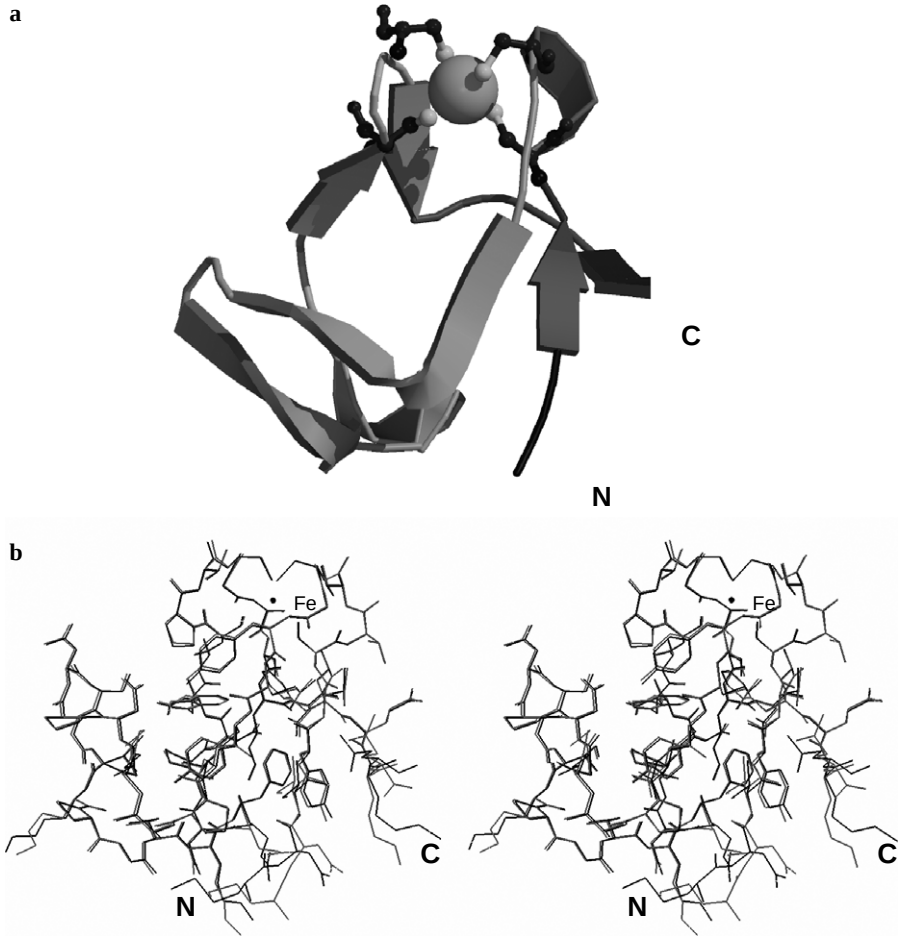

Fig. 3. (a) Ribbon drawing of Rd structure with MOLSCRIPT (Kraulis, 1991). The iron atom (as a ball) is bound in a tetrahedral coordination by the sulfur atoms of four cysteinyl residues (as ball and stick) at the two pairs of anti-parallel strands. (b) Superimposed Rd structures of 1.4-Å resolution (grey line) and 0.68 Å resolution (in black line) show the similar folding with major structural differences on the terminals and Asp-35.

high resolution structure reveals several multiple side-chain conformations of the residues Valine and Proline (Fig. 6). In addition, the solvent molecules and small molecules of crystallization chemicals, e.g., $(NH_4)_2SO_4$, appeared much more clearly on the maps of electron density at this resolution (Fig. 5). The 1.4 Å resolution structure contained 80 water molecules with fully occupied sites, whereas 101 solvent molecules were located in the ultrahigh-resolution structure. As shown in Fig. 7, the electron density map demonstrates that the geometry about the iron ion is essentially tetrahedral. Fig. 7 shows a comparison of bond distances (Fe—SG), angles (SG–Fe–SG'), and temperature factors (SG atoms) of the iron–sulfur cluster between Rd structures at 0.68 Å and 1.4 Å resolution. The cluster feature is essentially the same but with notable differences, such as 2.33 and 2.27 Å for the distance Fe-39SG for 0.68 Å and 1.4 Å resolution. The temperature factors of SG atoms of four cysteinyl residues are smaller for 0.68 Å resolution (averaged 4.3 $Å^2$) than for 1.4 Å resolution (averaged 6.4 $Å^2$) structures. Moreover, some H atoms appeared clearly on the $|F_o - F_c|$ density map at the 3.0-σ level, which provides direct evidence for hydrogen bonding. Fig. 8 shows the positions of the H atoms of Cys9N at the 3.5-σ level. With considerable variety in the primary structures, redox potentials, net overall charges, and sizes of Rds from different species, their iron-cluster structures are highly conserved, and the folding in the vicinity of the cluster is similar. It thus becomes important to understand the structural basis at the ultrahigh-resolution level for the differences in redox potential of electron transfer proteins. The comparison of these heterologous proteins with their respective residue changes provides a possibility to determine some general rules concerning the structure of other rubredoxins for which the amino acid sequence has been determined and in mapping the recognition sites of NRO, ROO, and other redox partners.

Iron environment

The two pairs of antiparallel strands comprising residues 3–13 and 36–46 form two hydrophobic arms (related by an approximate 2 fold axis), which hold the iron atom through four cysteinyl ligands. The iron center is located in the molecule in a region surrounded by hydrophobic residues. The Fe—SG bond lengths differ insignificantly; the SG–Fe–SG angles deviate slightly from tetrahedral values but remain

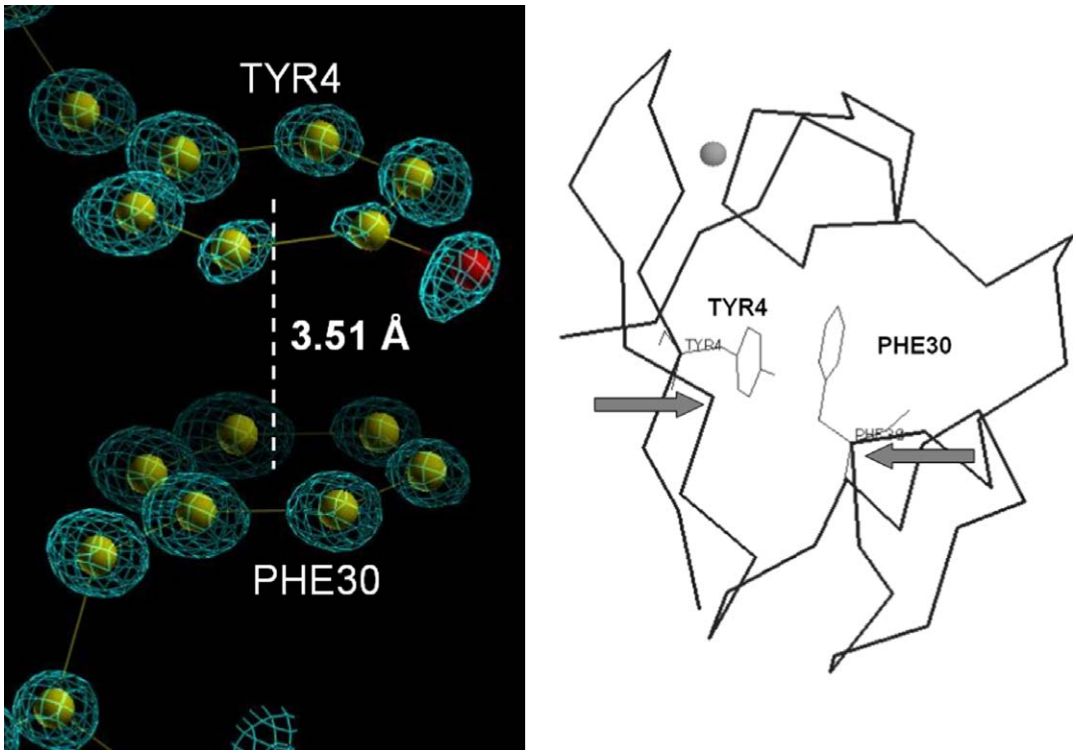

Fig. 4. σ-weighted $|2F_o - F_c|$ density map (4σ, cyan). Hydrophobic and π–π interaction maintain the internal Rd folding. A possible role of aromatic core is to mediate a long-range electron transfer, through π–π interactions, between the redox center and a functional partner, which would interact with rubredoxins on the opposite side of the molecule.

related by the twofold axis. The torsion angles, defined by CA-CB-SG-Fe, which are coupled to the breathing modes of the Fe—SG4 array, have values near 90° or 180°. The immediate environment of the iron also includes a dense network of hydrogen bonds such as N—H···SG described by Adman et al. [38]. The sulfur atoms SG6 and SG39 are involved in two such bonds, and SG9 and SG42 in just one. Taking advantage of ultrahigh-resolution data, we observe the electron density of hydrogen bond between SG6 and N9 as in Fig. 8. The hydrogen bond distances and angles among the iron–sulfur cluster of *D.g.* Rd at 0.68 Å and 1.4 Å resolution are shown in Fig. 8.

Due to the target values and the restraints used in the different refinement of other Rd crystal structures at their corresponding resolutions (1.8–1.0 Å), the accuracy of these individual values should not be overemphasized. Hence, the values from the structure at 0.68 Å resolution can provide the best reference and indication among all Rds. The N—H···SG bonds of SG6 to the backbone amides of 8 and 9 and the one from SG9 to N11 are on one side of the twofold axis symmetry whereas the N—H···SG bonds of SG9 to the amides of 41 and 42 and SG42 to the amide of 44 are on the other side of that symmetry. The ultra-high resolution data confirm the interesting pattern of N—H···SG bonds that SG with two N—H···SG bonds have longer Fe—S bonds (lengths 2.34 and 2.33 Å) whereas the SG with the single N—H···SG bond have shorter Fe—S bonds (lengths 2.31 and 2.30 Å) (Fig. 7). Furthermore, careful inspection of N-HSG bond distances relative to the local pseudo-twofold axis among the listed oxidized Rds clearly shows that this symmetry is broken down by means of average values and the 0.68-Å resolution data.

Fig. 8 shows the excellent quality of sigma-weighted $|2F_o–F_c|$ electron density at a resolution of 0.68 Å about the Fe—4Cys center, which allows one to assign the atom positions accurately. Interestingly, the $|F_o–F_c|$ difference Fourier map shows the extra density (over 4 σ) about the Fe and four SG atoms. The extra densities of Fe, SG6, SG42, and SG39 are distributed in the same direction whereas the larger extra density of SG9 is distributed in the different direction. Thus, SG9 and SG42 densities move toward the Fe atom whereas SG6 and SG39 densities shift away from the Fe atom. This atypical phenomenon might explain the reason why the bond lengths of Fe—SG6 (2.34 Å) and Fe—SG39 (2.33 Å) are longer than those of Fe—SG9 (2.31 Å) and Fe—SG42 (2.30 Å). The direction of density movement might imply the dynamic range of the Fe—4Cys center, which is related to the electron transfer mechanism.

Solvent molecules

Solvent molecules, which are bound to all polar atoms exposed to the external medium, cover nearly the entire surface of the protein (Fig. 5). The ones ordered best bind to peptide HN groups to stabilize either the molecular structure itself, or the intermolecular packing, or both.

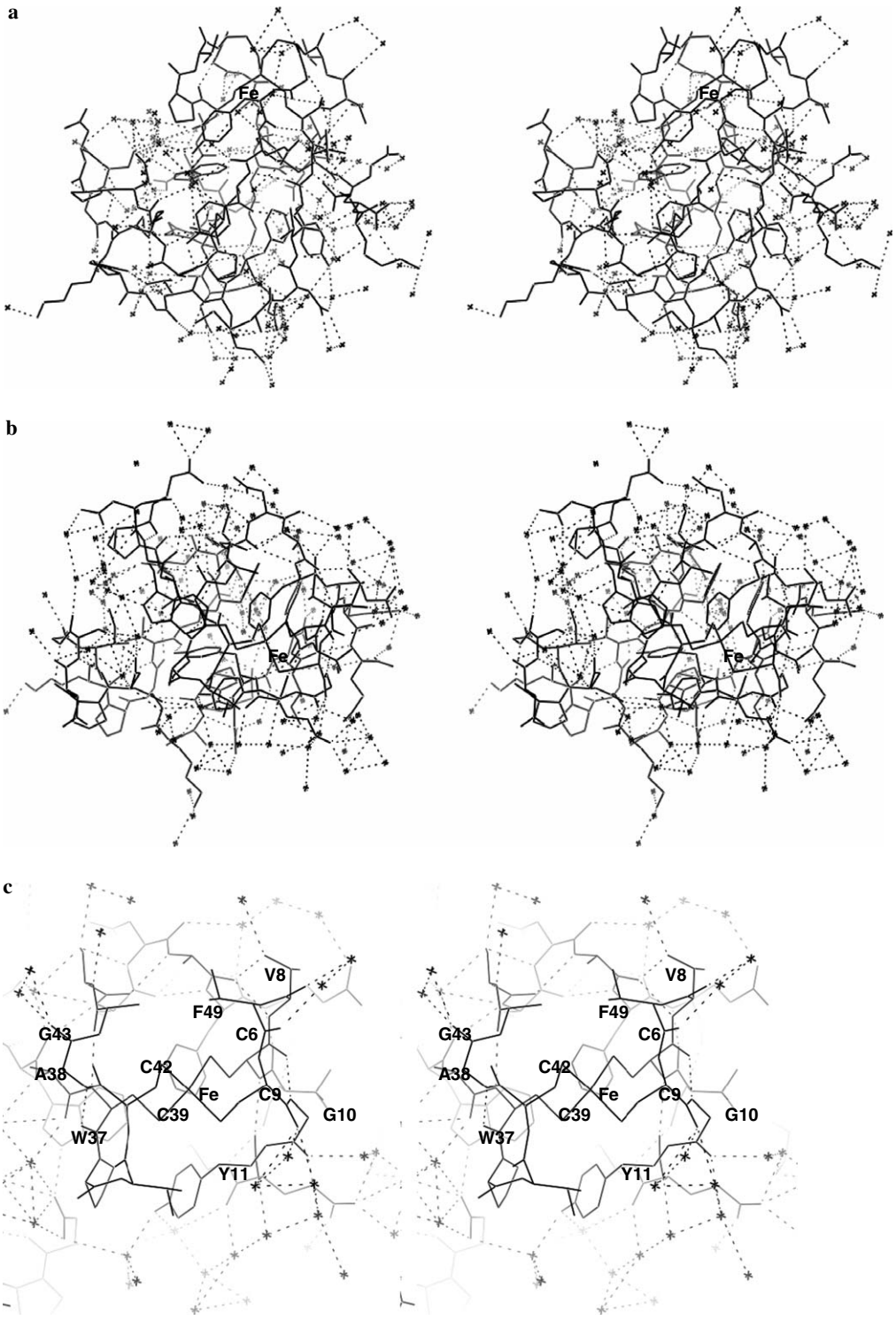

Fig. 5. An overall stereo view of the hydrogen bonding network of solvent–protein, solvent–solvent protein–protein interactions; (A) view from the same orientation as Fig. 2; (B) view from the 90°-rotated orientation; (C) a close view of Fe-4Cys redox center showing the abundant waters bound to C-O peptides of residues Val8, Cys9, Gly10, Ala38, and Gly43, which may be involved in electron transfer.

From the solvent content (27%) one can predict 94 theoretical solvent sites, in total, in the asymmetric unit. 101 possible sites have been included in the refinement, but five of them have no direct contacts with the protein ($d > 4.1$ Å). The well-ordered structural solvent molecules are generally found in nearly identical positions in RdDg at 1.4 Å resolution. Two of them are buried within the molecule and appear to be essential in maintaining the folding, for they contribute to stabilize loops of the protein: Pro15 to Gly27.

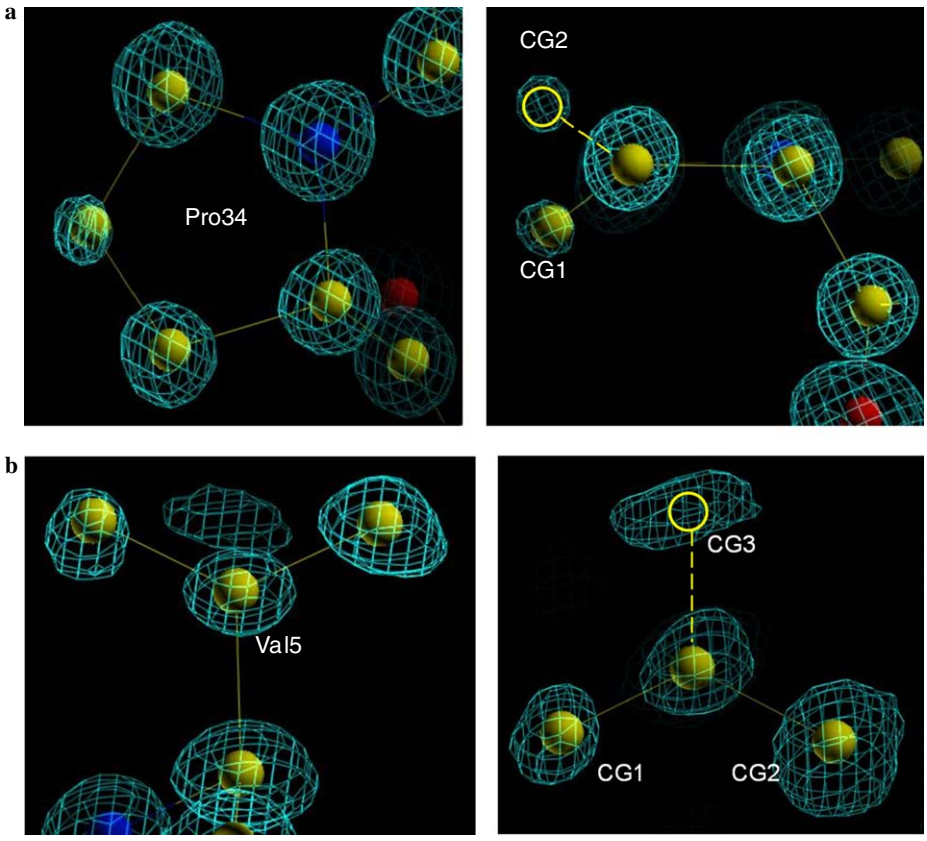

Fig. 6. σ-weighted omitted $|2F_o - F_c|$ density map (4σ, cyan). (a) Pro34, the *B*-factor value for CG1 is 5.74 Å^2 and for CG2 is 5.79 Å^2. (b) Val5, the *B*-factor value for CG1 is 4.34 Å^2, for CG2 is 6.63 Å^2, and for CG3 is 10.42 Å^2.

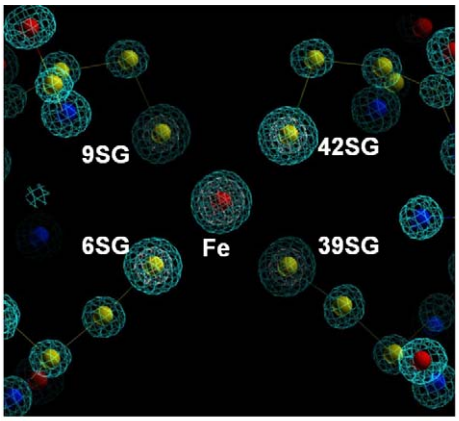

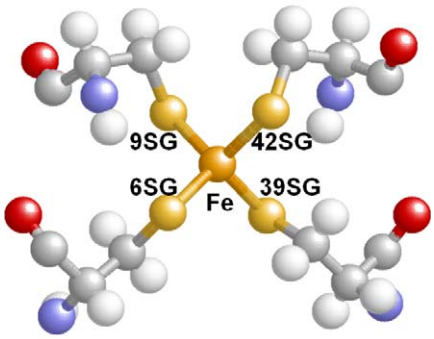

Distance (Å) & B(Å^2) of Fe-SG atoms		
Fe-6SG	2.34 (2.31)	3.9 (5.6)
Fe-9SG	2.31 (2.30)	4.5 (7.2)
Fe-39SG	2.33 (2.27)	4.3 (6.2)
Fe-42SG	2.30 (2.27)	4.4 (6.6)

Angles (°)	
6SG-Fe-9SG	114 (115)
6SG-Fe-39SG	110 (111)
6SG-Fe-42SG	105 (106)
9SG-Fe-39SG	104 (103)
9SG-Fe-42SG	112 (110)
39SG-Fe-42SG	112 (112)

Fig. 7. Structural comparison of the iron–sulfur redox center; the values for 1.4 Å structure (Frey et al., 1987) are indicated in parentheses.

Redox properties

For intramolecular electron transfer, the role of the N—H···SG bond network in accommodating the iron atom within the protein is described, but its involvement in electron transfer remains uncertain. This network may transfer charges from the iron–sulfur cluster to the coupled carbonyl oxygen atoms O7, O8, O10, O40, O41, and O43,

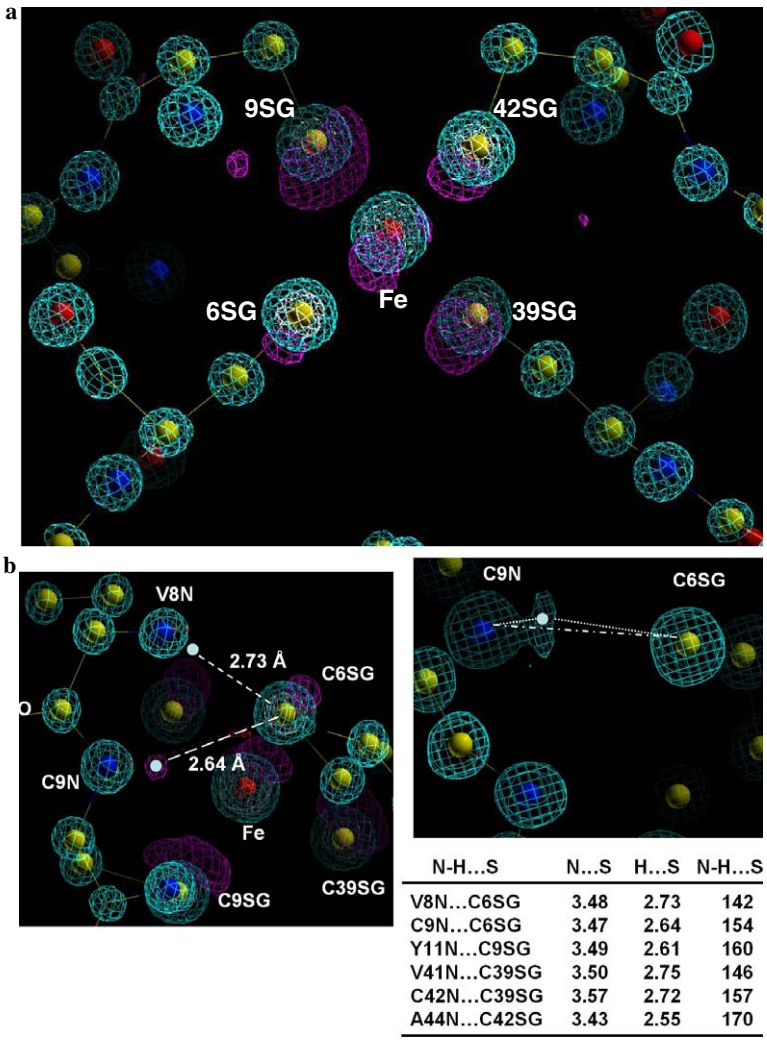

N-H…S	N…S	H…S	N-H…S
V8N…C6SG	3.48	2.73	142
C9N…C6SG	3.47	2.64	154
Y11N…C9SG	3.49	2.61	160
V41N…C39SG	3.50	2.75	146
C42N…C39SG	3.57	2.72	157
A44N…C42SG	3.43	2.55	170

Fig. 8. Distribution of electron density of the Fe-CYS4 environment. (a) σ-weighted $|2Fo\text{-}Fc|$ (4σ, cyan; 16σ, white) and $|Fo\text{-}Fc|$ (4σ, magenta) maps show the movement of the tendency of electron density that might imply the dynamics and uneven electron distribution around the cluster. (b) At resolution 0.68 Å, hydrogen atoms and bonding are clearly revealed. The network might transfer charges from the cluster to the coupled carbonyl oxygen atoms.

which are exposed to the solvent (Fig. 5). The exclusion of the FeSG4 redox center from solvent appears related to a positive shift of the redox potential, which is consistent with high redox potentials of rubredoxins, the values of which, like those of monohemic cytochrome c553 from *D. vulgaris*, are the most positive (about 0 mM for RdDg and −57 mV for RdCp) found among redox carriers in sulfate-reducing bacteria. A possible role of the aromatic core is involved in mediating long-range electron transfer, through π–π interactions, between the redox center and a functional partner, which would then interact with rubredoxins on the opposite side of the molecule.

For intermolecular electron transfer, a probable recognition pattern between the rubredoxin and its functional partners implies the following: a close approach to the redox centers; a topological complementarity of nearby hydrophobic regions of the surface, and specific interactions between surrounding residues that are oppositely charged—some of these being sequence invariants. The residues of the acidic ring of solvent-exposed residues found around FeSG4 appear to be the best candidates for possible recognition sites. The specificity might then be modulated by their distribution among several topologically close sites (e.g., residues 5, 12, and 50). In contrast, residues farther from the FeSG4 array could possibly be involved in the recognition process with regards of small molecular weight of rubredoxins relative to those of reductases, which implies that the rubredoxin molecule would be somehow embedded in the reductase.

Although rubredoxin was discovered as early as 1972 [39] in *Desulfovibrio*, only in 1993 [16] could we clearly demonstrate its involvement in the reduction of oxygen by *D. gigas*. The role of this protein is not well-established in other *Desulfovibrio* species and, to our knowledge, in any other anaerobe. The paradox is that the structure of rubredoxin is one of the best known and that hundreds of publications have been dedicated to its properties. To understand the nature of the electron-transfer specificity among these proteins and to try to identify putative relevant residues involved in this interaction, a panel of mutants was generat-

ed by site-directed mutagenesis; they were purified and characterized by mass spectrometry, UV–visible spectrophotometry, redox titration, EPR, and anaerobic determination of their rates of reduction by NRO in the presence of NADH. Among them, remarkable variations in the redox potentials and the rates of reduction were observed, particularly for W37 (Trp37 was deleted), A48E, V8N, and Rd loop (seven amino acids between residues 22 and 30 were deleted). The mutants V8N and Rd loop show that the amino acid substitutions might increase the water accessibility (unpublished result). This Rd structure at ultrahigh-resolution 0.68 Å provide useful information and allows us to compare and study the relationship between structural changes, redox potential and solvent accessibility.

Coordinates

Atomic coordinates for the crystal structures of rubredoxin from *Desulfovibrio gigas* as described in this paper have been deposited in the Protein Data Bank (Accession Code 2DSX).

Acknowledgments

This work is dedicated to Prof. Jean Le Gall. We are grateful to our colleagues, Drs. Yuch-Cheng Jean and Chun-Shiun Chao and supporting staffs for the technical assistance of synchrotron radiation X-ray facility on data collection at BL13B of NSRRC in Taiwan, and Yu-San Huang and Kuan-Li Yu at BL12B2 of SPring-8 in Japan. This study was supported in part by the National Synchrotron Radiation Research Center 924RSB02 & 934RSB02 (CJC), 944RSB05 (MYL) and National Science Council NSC 94-2321-B-213-001 in Taiwan to C.-J. Chen.

References

[1] W. Lovenberg, B.E. Sobel, Ruberedoxin: a new electron transfer protein from *Clotridium pasteurinum*, Proc. Natl. Acad. Sci. USA 54 (1965) 193–199.

[2] S.W. Ragsdale, L.G. Ljungdahl, Characterization of ferredoxin, flavodoxin, and rubredoxin from *Clostridium formicoaceticum* grown in media with high and low iron contents, J. Bacteriol. 157 (1984) 1–6.

[3] S. Seki, A. Ikeda, M. Ishimoto, Rubredoxin as intermediary electron carrier for nitrate reduction by NAD(P)H in *Clostridium perfringens*, J. Biochem. 103 (1998) 583–584.

[4] L.C. Sieker, R.E. Stenkemp, J. LeGall, Rubredoxin in crystalline state, Method Enzymol. 243 (1994) 203–216.

[5] S.W. Ragsdale, L.G. Ljungdahl, D.V. DerVartanian, Isolation of carbon monoxide dehydrogenase from *Acetobacterium woodi* and comparisom of its properties with those of the *Clostridium thermoaceticum* enzyme, J. Bacteriol. 155 (1982) 1224–1237.

[6] H. Aurisch, D. Sorger, O. Asperger, Isolierung und charakterisieung eines rubredoxin aus *Acinetobacter calcoacetucus*, Acta Biol. Med. Germ. 35 (1976) 443–451.

[7] J.A. Peterson, M.J. Coon, Enzymatic omega-oxidation. 3. Purification and properties of rubredoxin, a component of the omega-hydroxylation system of *Pseudomonas oleovorans*, J. Biol. Chem. 243 (1968) 329–334.

[8] J.A. Peterson, M. Kusunose, E. Kusunose, M.J. Coon, Enzymatic ω-oxidation.II. Function of rubredoxin as the electron carrier in ω-hydroxylation, J. Biol. Chem. 242 (1967) 4334–4340.

[9] J. Le Gall, D.V. DerVartanian, H.D. Peck Jr., Flavoproteins, iron proteins and hemoproteins as Electron-transfer components of the sulfate reducing bacteria, Curr. Top. Bioenerg. 9 (1979) 237–265.

[10] J. Le Gall, J.J.G. Moura, H.D. Peck Jr., A.V. Xavier, Hydrogenase and other non-sulfur proteins from sulfate reducing and methane forming bacteria, in: T. Spiro (Ed.), Iron Sulfur Proteins IV, J. Wiley and Sons, New York, 1982, pp. 177–247.

[11] M. Bruschi, The amino acid sequence of rubredoxin from the sulfate reducing bacterium, *Desulfovibrio gigas*, Biochem. Biophys. Res. Commun. 70 (1976) 615–621.

[12] J.C. Chen, L.E. Mortenson, Identification of six open reading frames from a region of the *Azotobacter vinelandii* genome likely involved in dihydrogen metabolism, Biochim. Biophys. Acta 1131 (1992) 199–202.

[13] J. Le Gall, A.V. Xavier, Anaerobe response to oxygen: the sulfate-reducing bacteria, Anaerobe 2 (1996) 1–9.

[14] H. Santos, P. Fareleira, A.V. Xavier, L. Chen, M.-Y. Liu, J. Le Gall, Aerobic metabolism of carbon reserves by the "obligate anaerobe" *Desulfovibrio gigas*, Biochem. Biophys. Res. Commun. 195 (1993) 551–557.

[15] L. Chen, M.-Y. Liu, J. LeGall, P. Fareleria, H. Santos, A.V. Xavier, Purification of characterization of an NADH-rubredoxin oxidoreductase involved in the utilization of oxygen by *Desulfovibrio gigas*, Eur. J. Biochem. 216 (1993) 443–448.

[16] L. Chen, M.-Y. Liu, J. LeGall, P. Fareleira, H. Santos, A.V. Xavier, Rubredoxin oxidase, a new flavor-heme-protein, is the site of oxygen reduction to water by the "strict anaerobe" *Desulfovibrio gigas*, Biochem. Biophys. Res. Commun. 193 (1993) 100–105.

[17] G.M. Gomes, G. Silva, S. Oliveira, J. LeGall, M.-Y. Liu, A.V. Xavier, C. Rodrigues-pousada, M. Teixeira, Studies on the rudox centers of the terminal oxidase from *Desulfovibrio gigas* and evidence for interaction with rubredoxin, J. Biol. Chem. 272 (1997) 22502–22508.

[18] C. Frazao, G. Silva, C.M. Gomes, P. Matias, R. Coelho, L.C. Sieker, S. Macedo, M.-Y. Liu, S. Oliveira, M. Teixeira, A.V. Xavier, C. Rodrigues-Pousada, M.A. Carrondo, J. LeGall, Structure of dioxygen reduction enzyme from *Desulfovibrio gigas*, Nat. Struct. Biol. 17 (2000) 1041–1045.

[19] J.R. Herriott, L.C. Sieker, L.H. Jensen, W. Lovenberg, Structure of rubredoxin: an X-ray study to 2.5 Å resolution, J. Mol. Biol. 50 (1970) 391–402.

[20] M. Pierrot, R. Haser, M. Frey, M. Bruschi, J. LeGall, L.C. Sieker, L.H. Jensen, Some comparisons between two crystallized anaerobic bacterial rubredoxins from *Desulfovibrio gigas* and *D. vulgaris*, J. Mol. Biol. 107 (1976) 179–182.

[21] Z. Dauter, K.S. Wilson, L.C. Sieker, J.M. Moulis, J. Meuer, Zinc-and iron-rubredoxins from *Clostridium pasteurianum* at atomic resolution: a high-precision model of a ZnS4 coordination unit in a protein, Proc. Natl. Acad. Sci. USA 93 (1996) 8836–8840.

[22] M. Frey, L.C. Sieker, F. Payan, R. Haser, M. Bruschi, G. Pepe, J. LeGall, Rubredoxin from *Desulfovibrio gigas*. A molecular model of the oxidized form at 1.4 Å resolution, J. Mol. Biol. 197 (1994) 524–525.

[23] R.E. Stenkamp, L.C. Sieker, L.H. Jensen, The structure of rubredoxin from *Desulfovibrio desulfuricans* strain 27774 at 1.5 Å resolution, Proteins 8 (1990) 352–364.

[24] Z. Dauter, L.C. Sieker, K.S. Wilson, Refinement of rebredoxin from *Desulfovibrio vulgaris* at 1.0 Å with and without restraints, Acta Cryst. B48 (1992) 42–59.

[25] R. Bau, D.C. Rees, D.M. Kurtz, R.A. Scott, H. Huang, M.W.W. Adams, M.K. Eidsness, Crystal structure of rubredoxin from *Pyrococcus furiosus* at 0.95 Å resolution, J. Biol. Inorg. Chem. 3 (1998) 484–490.

[26] H. Bönishch, C.L. Schmidt, P. Bianco, R. Ladenstein, Ultrahigh-resolution study on *Pyrococcus abyssi* rebredoxin. I. 0.69 Å X-ray structure of mutant W4L/R5S, Acta Cryst. D 61 (2005) 990–1004.

[27] J. LeGall, G. Mazza, N. Dragoni, Cytochome c3 of *Desulfovibrio gigas*, Biochim. Biophys. Acta 99 (1965) 385–387.
[28] C.-J. Chen, M.-Y. Liu, Y.-T. Chen, J. LeGall, Preparation and X-ray crystallographic analysis of rubredoxin crystals from *Desulfovibrio gigas* to beyond ultra-high 0.68 Å resolution, Biochem. Biophys. Res. Commun. 308 (2003) 684–688.
[29] Z. Otwinowski, W. Minnor, Processing of X-ray diffraction data collected in oscillation mode, Methods Enzymol. 276 (1997) 307–326.
[30] T.C. Terwilliger, J. Berendzen, Automated MAD and MIR structure solution, Acta cryst. D 55 (1997) 849–861.
[31] G.M. Sheldrick, T.R. Schnider, SHELX: high-resolution refinement, Methods Enzymol. 277 (1997) 319–343.
[32] A.T. Brünger, P.D. Adams, G.M. Clore, W.L. DeLano, P. Gros, R.W. Grosse-Kunstleve, J.-S. Jiang, J. Kuszewski, N. Nilges, N.S. Pannu, R.J. Read, L.M. Rice, T. Simonson, G.L. Warren, Crystallography & NMR system: A new software suite for macromolecular structure determination, Acta Cryst. D 54 (1998) 905–921.
[33] T.A. Jones, J.-Y. Zou, S.W. Cowan, M. Kjeldgaard, Improved methods for building protein models in electron density maps and the location of errors in these models, Acta Cryst. A 47 (1991) 110–119.
[34] Collaborative Computational Project, Number 4, The CCP4 suite: programs for protein crystallography, Acta Cryst. D 50 (1994) 760-763.
[35] V. Luzzati, Traitement statistique des erreurs dans la determination des structures crystallines, Acta Cryst. 5 (1952) 802–810.
[36] M.W. MacArthur, J.M. Thornton, Deviations from planarity of the peptide bond in peptides and proteins, J. Mol. Biol. 264 (1996) 1180–1195.
[37] J.S. Richardson, in: C.B. Anfinsen, J.T. Edsall, F.M. Richards (Eds.), Advances in Protein Chemistry, vol. 34, Academic Press, New York, 1981, pp. 167–339.
[38] E.T. Adman, K.D. Watenpaugh, L.H. Jensen, NH-S hydrogen bonds in *Peptococcus aerogenes* ferredoxin, *Clostridium pasteurianum* rubredoxin, and *Chromatium* high potential iron protein, Proc. Natl. Acad. Sci. USA 72 (1975) 4854–4858.
[39] M. Bruschi, J. Le Gall, Purification et propriétés d'une rubrédoxine isolée à partir de *D. vulgaris* (souche NCIB 8380), Biochim. Biophys. Acta 263 (1972) 279–282.